

pubs.acs.org/JPCL Letter

Halide Vacancies Create No Charge Traps on Lead Halide Perovskite Surfaces but Can Generate Deep Traps in the Bulk

Jingyi Ran, Bipeng Wang, Yifan Wu, Dongyu Liu, Carlos Mora Perez, Andrey S. Vasenko, and Oleg V. Prezhdo*



Cite This: J. Phys. Chem. Lett. 2023, 14, 6028-6036



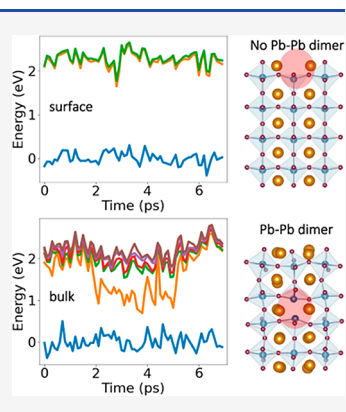
ACCESS I

III Metrics & More

Article Recommendations

Supporting Information

ABSTRACT: Metal halide perovskites (MHPs) have attracted attention because of their high optoelectronic performance that is fundamentally rooted in the unusual properties of MHP defects. By developing an ab initio-based machine-learning force field, we sample the structural dynamics of MHPs on a nanosecond time scale and show that halide vacancies create midgap trap states in the MHP bulk but not on a surface. Deep traps result from Pb—Pb dimers that can form across the vacancy in only the bulk. The required shortening of the Pb—Pb distance by nearly 3 Å is facilitated by either charge trapping or 50 ps thermal fluctuations. The large-scale structural deformations are possible because MHPs are soft. Halide vacancies on the MHP surface create no deep traps but separate electrons from holes, keeping the charges mobile. This is particularly favorable for MHP quantum dots, which do not require sophisticated surface passivation to emit light and blink less than quantum dots formed from traditional inorganic semiconductors.



etal halide perovskites (MHPs) have garnered signifietal name perovantes (manager)

cant attention as solar cell candidates due to their low manufacturing cost and versatile electronic and optical properties, 1,2 including a tunable band gap, 3-5 long charge carrier diffusion, 6-9 and strong light absorption. 10-12 With these exceptional characteristics, MHPs can achieve solar-toelectricity conversion efficiencies of >25%, 13 approaching or even surpassing those of traditional semiconductors such as silicon. Furthermore, MHPs are much more diverse than traditional semiconductors, owing to the versatile perovskite structure that allows a broad range of compositions and dimensionalities. 14-17 MHPs are softer than inorganic semiconductors and undergo significant structural fluctuations that can lead to large fluctuations of electronic energy levels, particularly those associated with defects. 18-21 During the fluctuations, midgap trap states can appear, reducing the energy gap between the highest occupied molecular orbital (HOMO) and the lowest unoccupied molecular orbital (LUMO). The HOMO and LUMO can split off the valence and conduction bands and form midgap trap states that can capture charge carriers, affecting their transport and recombination. 22-27 The energy level fluctuations in MHPs are much more significant than those in the traditional inorganic semiconductors, 18 and such fluctuations contribute to the unusual defect properties of MHPs. $^{26-32}$ Defects in MHPs and their fluctuations have been extensively studied at the ab initio level. However, ab initio calculations are typically limited to picoseconds, while MHPs undergo much slower structural oscillations and rearrangements. To gain a thorough understanding of the MHP properties, it is essential to develop

atomistic models that can sample MHP conformations on time scales similar to charge carrier lifetimes. Extending the studies to hundreds of picoseconds has already revealed new dynamic regimes and phenomena. ^{19–21,33}

Machine-learning (ML) techniques allow one to train force field (FF) models utilizing data from ab initio methods and then apply MLFFs to sample a broad range of atomic geometries and long time scales. MLFF algorithms offer high accuracy while reducing computational cost compared to calculations relying solely on ab initio methods.^{34–37} MLFFs allow one to address many problems, such as anharmonic lattice dynamics, ^{38,39} phase transitions, ^{40,41} chemical dynamics, ^{42,43} etc. ^{20,21,44} Structural motifs in condensed matter systems enable the generation of global and local descriptors. These mathematical representations capture essential features of a system and can be used to create physically motivated FF models that approximate accurately interactions between particles. 45 As a result, cost-effective MLFFs can facilitate molecular dynamics (MD) simulations for larger MHP systems with longer trajectories compared with those of ab initio MD simulations. MLFF-assisted studies can provide insights into the structural evolution of MHPs on nanosecond time scales, comparable to those of charge carrier trapping and

Received: May 6, 2023 **Accepted:** June 12, 2023 **Published:** June 23, 2023





recombination. Then, ab initio methods can be used to sample electronic structure and electron—vibrational interactions, providing important insights into how slow geometry fluctuations influence excited state dynamics that govern material properties and determine device efficiencies.

In this Letter, we demonstrate that a halide vacancy, one of the most common defects in MHPs, 46,47 exhibits different behavior on the surface and in the bulk. Focusing on the Br vacancy in CsPbBr3, we develop a MLFF that allows us to sample MHP structural dynamics on a nanosecond time scale and identify changes in the electronic properties induced by such dynamics. At 0 K, neither bulk nor surface vacancy exhibits midgap levels. However, at ambient temperature, up to four midgap trap states can emerge on a time scale of tens of picoseconds in the bulk but not on the surface. Similarly, charging the vacancy can create deep traps only in the bulk. The defect level properties correlate well with the distance between the two Pb atoms surrounding the bulk vacancy. In contrast, for the surface vacancy, no correlations are observed between the movement of the Pb atom directly beneath the vacancy and the energy of the electronic state. Rather than trapping charges, the surface halide vacancy facilitates electron-hole separation while keeping charges mobile. The deep traps appear in the bulk only transiently and infrequently, and therefore, they are not detrimental to optoelectronic performance. However, once charged, the traps become stable and can cause poorer performance, e.g., at a high carrier density. The absence of charge traps due to halide vacancies on the MHP surface rationalizes the excellent optoelectronic properties of perovskite quantum dots (QDs), which emit well and blink little, in comparison to QDs composed of traditional inorganic semiconductors that blink due to surface charge trapping.

Density functional theory (DFT) calculations are performed using the Vienna Ab-initio Simulation Package (VASP).⁴⁸ The electron-ion interactions are characterized by employing the Perdew-Burke-Ernzerhof (PBE) functional⁴⁹ and the projector-augmented-wave (PAW) method.⁵⁰ A 400 eV plane-wave energy cutoff is used. The structures are visualized using the VESTA software. 51 Two CsPbBr3 models with Br vacancies on the surface and in the bulk are constructed by considering a CsPbBr₃ slab composed of $2 \times 2 \times 5$ unit cells (Figure 1). The surfaces of the slab are terminated with CsBr, because such termination provides the most stable surfaces, as established both experimentally^{52,53} and theoretically.^{54,55} A 20 Å vacuum layer is added to the z-direction containing five-unit cells. Periodic boundary conditions are employed in all directions. Br vacancies are introduced by removing one Br atom from the top (surface) and middle (bulk) layers. The locations of these vacancies are highlighted by the dotted green circles in panels a and d of Figure 1. The electronic structure calculations are performed at the Γ k-point because the structure already includes 20-unit cells and because the CsPbBr3 band gap is located at the Γ point. The CsPbBr₃ models with Br vacancies contained 87 atoms each.

To investigate the defect properties on a nanosecond time scale, which is comparable to the duration of charge carrier trapping and recombination, and to circumvent the high computational cost of direct ab initio calculations, a MLFF model is trained for the vacancy systems. For the collection of training and validation data sets, the CsPbBr₃ systems with the Br vacancies are heated from 0 to 1600 K in increments of 100 K using the ab initio method described above. The wide range

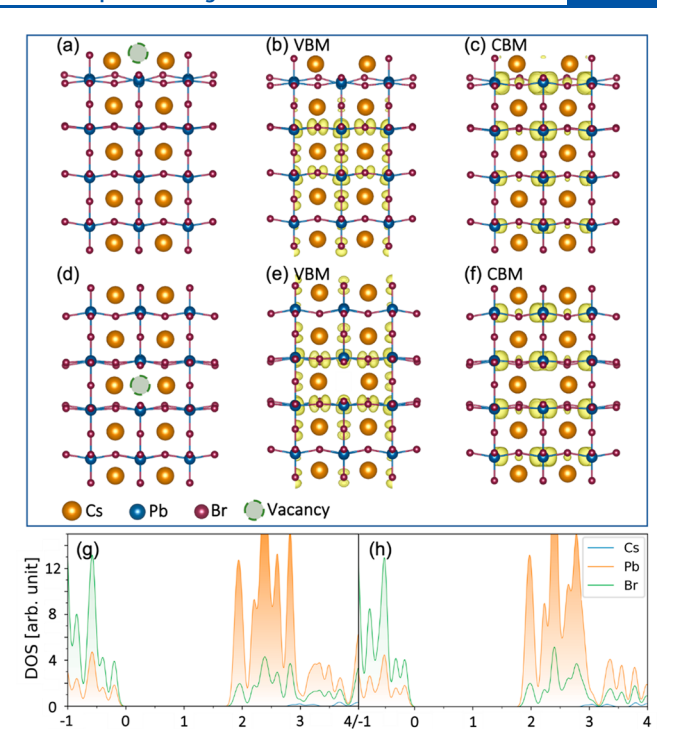


Figure 1. (a) Optimized structure of CsPbBr₃ with a Br vacancy on the surface. Cs, Pb, and Br are represented by large light brown, medium blue, and small dark brown spheres, respectively. The vacancy is highlighted by the green circle. (b and c) Corresponding VBM and CBM charge densities, respectively. (d) Optimized structure of CsPbBr₃ with the Br vacancy in the bulk. (e and f) Corresponding VBM and CBM charge densities, respectively. (g and h) Projected DOS of CsPbBr₃ with the Br vacancy on the surface and in the bulk, respectively, at 0 K. In the optimized structures, the vacancies create no midgap trap states, and the frontier orbitals are delocalized.

Energy [eV]

of temperatures provides a diverse set of configurations that the systems may explore on a long time scale at ambient temperature. At each temperature up to 1200 K, 4000 data points are collected, while 2000 data points are gathered at the higher temperatures. The output of the ab initio calculations is processed by a data preparation algorithm embedded in the DeepMD package⁵⁶ to extract information for the MLFF model's input data. The input data are randomly partitioned into training and validation sets at an approximate ratio of 80:20. The quality of the MLFF is assessed by comparing the potential energies obtained ab initio and from the ML model. The ML and ab initio potential energies show good agreement, as demonstrated in Figure S1. The root-mean-square errors are 1.74 meV per atom for the surface vacancy system and 2.18 meV per atom for the bulk vacancy system.

Once a reliable MLFF model is established, the systems are heated to 300 K, and 1 ns MD trajectories are generated for each system in the microcanonical ensemble, using the Large-scale Atomic/Molecular Massively Parallel Simulator (LAMMPS).⁵⁷ During the 1 ns MD trajectories, the Br vacancies are observed to migrate between layers, indicating that the MLFF method can be used to perform a detailed atomistic study of defect migration that plays important roles in MHPs, causing phase separation, current—voltage hysteresis, and chemical instabilities.^{58–62} For the purpose presented here, we select parts of the trajectories in which the vacancies remain

in the selected locations. Once the MLFF trajectories are generated, the electronic properties are investigated every 1 ps by ab initio DFT. The electronic properties for selected parts of the trajectories are investigated every 100 fs. The developed MLFF allows one to study large systems; however, the need to characterize the electronic properties for multiple geometries using ab initio DFT sets a limit on the system size.

Figure 1 presents the geometric and electronic structures of the defective $CsPbBr_3$ systems in the optimized geometries, corresponding to 0 K. The Pb–Pb distance surrounding the vacancy in the bulk is 6.19 Å, similar to that in the pristine region without vacancies. Despite the presence of the defects, no midgap trap states are observed in either structure. The charge densities of the valence band maximum (VBM) and conduction band minimum (CBM) for both surface and bulk vacancies are delocalized. The densities of states (DOS) for the two structures demonstrate that the CBM and VBM are formed primarily by Pb and Br atomic orbitals, respectively.

At ambient temperature, MHPs undergo significant structural fluctuations that can modulate their electronic properties. Defect levels that are either shallow or hidden inside bands at 0 K can become deep, while levels that are deep at 0 K can approach band edges. In particular, a halide vacancy defect that creates no midgap states in the optimized geometry can create a level as deep as 1 eV below the CBM at room temperature. 18,19 In this study, we observe a qualitative difference in the fluctuation of the defect energy levels for the Br vacancy on the surface and in the bulk. The surface vacancy is located on the topmost layer of the slab, while the bulk vacancy is in the middle of the slab (Figure 1). While both structures undergo significant geometric distortions at ambient temperature, only the bulk Br vacancy creates deep midgap trap levels. The Br vacancy on the CsPbBr3 surface creates no deep trap levels, though the band edges still undergo fluctuations (Figure S2).

Figure 2 presents the evolution of the energy gap between the lowest unoccupied molecular orbital (LUMO) and LUMO +1 for CsPbBr₃ with the Br vacancy in the bulk. The figure also shows the distance between the two Pb atoms across the vacancy. The evolution of the electronic energy levels from HOMO-5 to LUMO+5 is shown in Figure S2. There are several times over the 200 ps trajectory during which the LUMO/LUMO+1 energy gap reaches 0.6 eV, while LUMO separates from the CBM by 1 eV, like the iodine vacancy in bulk MAPbI₃. Focusing on one such event (Figure 2a), we observe that the deep trap exists for ~ 3 ps, also like MAPbI $_3$ with an iodine vacancy. ¹⁹ The LUMO/LUMO+1 energy gap exhibits a strong correlation with the Pb-Pb distance: the shorter the distance, the deeper the trap state. The Pb-Pb distance across the Br vacancy measures 6.19 Å in the optimized structure, while it fluctuates from 3.80 to 6.45 Å at 300 K. The 2.65 Å fluctuation of the defect structure, giving rise to the 1 eV fluctuation of the defect energy level, is possible because MHPs are soft, much softer than traditional inorganic semiconductors, such as Si, CdSe, and TiO2. When the Pb-Pb distance is at its shortest, up to four midgap states can appear (Figure 3).

Figure 3 demonstrates projected DOS for four representative CsPbBr₃ structures with the Br vacancy in the bulk, exhibiting one to four midgap states. The corresponding charge densities can be found in Figure 4 and Figure S3. Generally, the shorter the Pb–Pb distance, the greater the number of midgap states. When the Pb–Pb distance exceeds

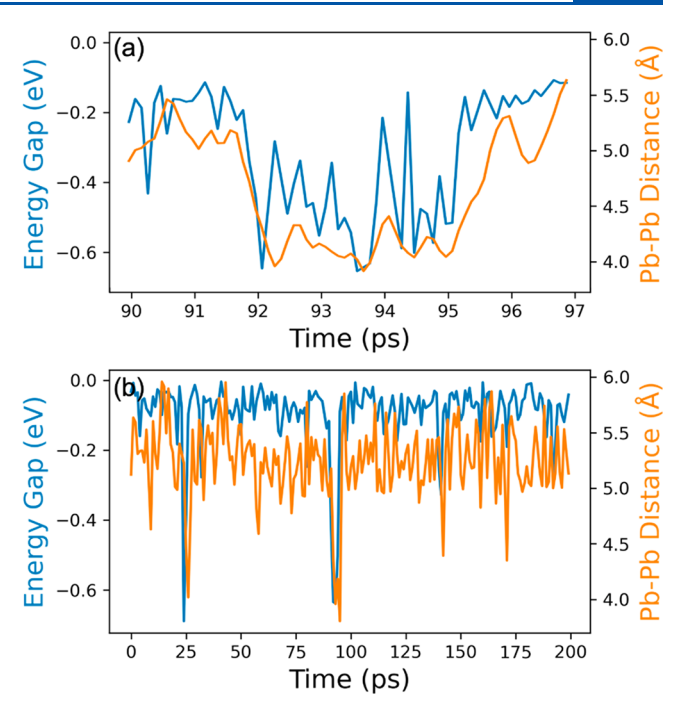


Figure 2. Correlation between the energy gap from LUMO to LUMO +1 (blue) and the Pb–Pb distance (orange) in CsPbBr₃ with the Br vacancy in the bulk for (a) a 7 ps region with a deep trap and (b) the long trajectory. The time period shown in panel a matches the time in panel b. A strong correlation is observed. The Pb–Pb distance refers to the two Pb atoms across the vacancy. The LUMO to LUMO+1 gap demonstrates that the deepest midgap trap state fluctuates by 0.6 eV away from the second deepest trap. Overall, the deepest trap fluctuates 1 eV down from the CsPbBr₃ CBM, as illustrated in Figure S2.

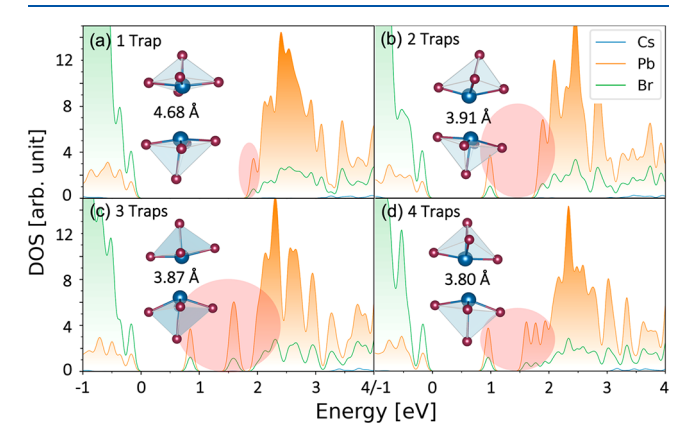


Figure 3. (a–d) Projected DOS of CsPbBr₃ with a Br vacancy in the bulk at four representative MD time points. Midgap trap states emerge as the Pb–Pb distance varies from 4.68 to 3.80 Å. A greater number of midgap trap states are observed as the Pb–Pb distance is shortened. When the Pb–Pb distance reaches 3.80 Å, four trap states are detected.

4.7 Å, no trap states are observed, as shown in Figure S4. As the Pb—Pb distance decreases, midgap trap states begin to emerge. Figure 3 illustrates a single trap appearing when the Pb—Pb distance reaches 4.68 Å and two traps emerging when the distance is reduced to 3.91 Å. Subsequently, three traps appear when the Pb—Pb distance reaches 3.87 Å, and four traps appear when the distance is 3.80 Å. A maximum of three trap states was observed in the previous study of the halide

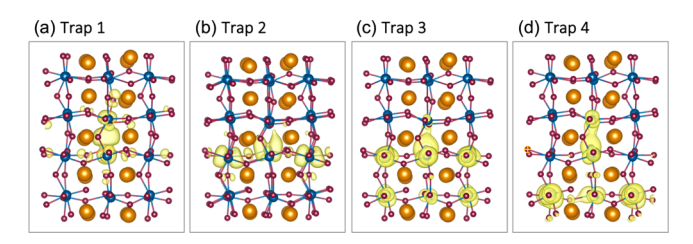


Figure 4. (a–d) Charge densities of the four midgap trap states in CsPbBr₃ with the Br vacancy in the bulk, corresponding to Figure 3d. All midgap states are localized around the vacancy. Trap 1 is supported by the σ -bond formed by two p orbitals of the Pb atoms across the vacancy. It has the lowest energy and is the most localized. The other trap states are supported by p orbitals perpendicular to the Pb–Pb dimer direction, forming π -bonds. They are higher in energy and delocalize onto neighboring pristine Pb atoms.

vacancy in MAPbI₃, ¹⁹ in comparison to the four states seen here. Most likely, this is because the CsPbBr3 structure is more compact than the MAPbI₃ structure, because Br is smaller than I and Cs is smaller than MA. Thus, shorter Pb-Pb distances are possible across the halide vacancy in CsPbBr3 than in MAPbI₃. All-inorganic perovskites, such as CsPbBr₃, differ from mixed organic-inorganic perovskites, such as MAPbI₃, in the shape of the inert cation Cs+ versus MA+. Cs+ and other inorganic cations are spherically symmetric, while MA+ and other organic cations have an asymmetric charge distribution and can form hydrogen bonds with the inorganic lattice.⁶³ These factors can create additional structural disorder in hybrid organic-inorganic perovskites compared to all-organic perovskites, increasing charge localization. 64-66 In both CsPbBr₃ and MAPbI₃ studied thus far, only one of the trap states arising from a halide vacancy is very deep, while the other states are relatively shallow (Figure 3 and ref 19).

Analysis of the defect state charge densities indicates that deeper traps are more localized (Figure 4 and Figure S3). Shallower traps couple strongly with CsPbBr₃ conduction band states and extend onto multiple neighboring atoms of the pristine structure. The missing Br atom leaves unsaturated valencies in the two surrounding Pb atoms, and the charge densities of the trap states are localized on the corresponding Pb orbitals. Table 1 presents the contributions of p orbitals from the two Pb atoms to the four traps seen in Figure 3d, with the charge densities shown in Figure 4. The deepest trap 1 is localized on the p_z orbitals of the two Pb atoms and is oriented perpendicular to the slab. Trap 2 is oriented in the plane of the slab. It originates from the p_z orbital of a single Pb atom and spreads onto the neighboring Pb atoms in the x-direction. Both

Table 1. Contributions of p Orbitals of the Two Pb Atoms across the Vacancy Site in CsPbBr₃ with the Br Vacancy in the Bulk, Corresponding to the Four Trap Charge Densities Shown in Figure 4

		p_x	\mathbf{p}_{y}	p_z
trap 1	Pb (above)	0.000	0.000	0.139
	Pb (below)	0.000	0.000	0.025
trap 2	Pb (above)	0.007	0.000	0.001
	Pb (below)	0.259	0.000	0.000
trap 3	Pb (above)	0.000	0.013	0.001
	Pb (below)	0.000	0.163	0.002
trap 4	Pb (above)	0.000	0.026	0.001
	Pb (below)	0.000	0.088	0.001

trap 3 and trap 4 have charge densities supported by the p_y orbitals of the two Pb atoms across the vacancy. They delocalize significantly onto many neighboring Pb atoms. Trap 1 is a deep state, because it is supported by a σ -bond formed by the two Pb p orbitals pointing toward each other across the vacancy. The other states are formed by Pb p orbitals pointing perpendicular to the Pb—Pb vacancy dimer direction and, therefore, can form only π -bonds and are higher in energy.

In contrast to the bulk vacancy, the Br vacancy on the CsPbBr₃ surface does not exhibit deep traps. The LUMO/LUMO+1 energy gap fluctuates within 0.15 eV (Figure 5),

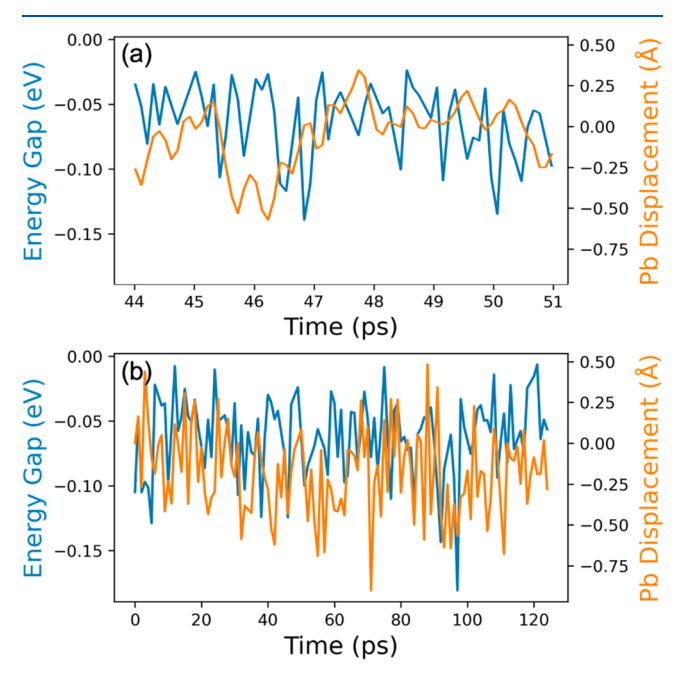


Figure 5. Relationship between the energy gap from LUMO to LUMO+1 and the displacement of the Pb atom under the Br vacancy on the CsPbBr₃ surface for (a) a selected 7 ps region and (b) the long trajectory. The time period shown in panel a matches the time in panel b. The Pb atom displacement refers to the position normal to the surface, and 0 refers to the average position of all Pb atoms in the surface layer. In contrast to the Br vacancy in the bulk, in **Figure 2**, the trap state separates from the CBM by only 0.15 eV, as illustrated further in **Figure S2**. No significant correlation between the energy gap fluctuation and the Pb movement is observed.

compared with the 1 eV fluctuation for the bulk vacancy (Figure 2). The HOMO/LUMO energy gap can decrease significantly (Figure S2c,e); however, this decrease is not associated with the formation of deep trap states separated from the bands. Rather, the whole set of valence and conduction band states fluctuate in energy, decreasing the fundamental band gap. It should be noted that, while the properties of defect states can be modeled with small models, such as the current simulation cell, because the defect states are localized, the extent of fluctuation of energies of delocalized band states may depend on simulation cell size, because typically, states delocalized over more atoms fluctuate less.

Halide vacancies on lead halide perovskite surfaces do not form deep trap states because there is only one Pb next to the vacancy and there is no opportunity to form a Pb—Pb dimer, as in the bulk. We did not find a simple structural feature that would correlate with the LUMO/LUMO+1 energy gap for the surface vacancy system. For example, considering the displace-

ment of the Pb atom below the vacancy in the vertical direction perpendicular to the slab, an analogue of the Pb—Pb dimer distance for a single Pb atom, we observe no correlation with the LUMO/LUMO+1 gap. Such a correlation should not be expected because defect states energetically close to band edges are coupled to band states and delocalize, and therefore, their properties are determined by collective motions of multiple atoms.

Figure 6 shows a representative CsPbBr₃ structure with the surface Br vacancy, its DOS, and charge densities of HOMO,

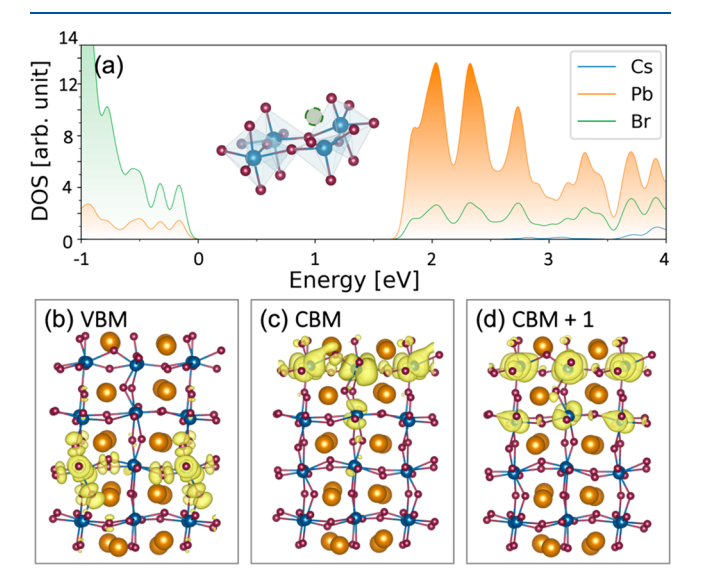


Figure 6. (a) DOS of CsPbBr₃ with the Br vacancy on the surface for a representative geometry at room temperature. (b-d) Charge densities of the VBM, CBM, and CBM+1, respectively. There are no midgap states. The VBM and CBM are spatially separated and remain largely delocalized. Such a condition favors long-lived excited states.

LUMO, and LUMO+1. Because there are no states inside the band gap separated energetically from the bands, the HOMO can be regarded as the VBM, and the LUMO as the CBM. All states are delocalized in the plane of the slab; however, the symmetry of the slab is broken by the vacancy, such that the CBM and VBM are localized on the opposite sides. Such a scenario leads to separation of electrons and holes, which nevertheless remain mobile because the HOMO and LUMO are delocalized and not separated from the bands energetically. Such a situation favors material performance in solar cells, detectors, and other applications that require charge separation. On the contrary, light-emitting diodes and lasers require the formation of excitons, i.e., bound electron-hole pairs, to emit light. Localization of the CBM and VBM on opposite surfaces is not maintained continuously. However, it assists in solar energy applications even if it happens only in a fraction of conformations. Such electron-hole symmetry breaking has been detected in other MHP systems, with and without defects.^{67–72} The reduced probability of formation of deep trap states on MHP surfaces and the electron-hole separation facilitated by surfaces, interfaces, and grain boundaries minimize nonradiative charge recombination that constitutes the primary loss channel in photovoltaic applications.

Calculations show that halide vacancies create midgap trap states associated with Pb—Pb bonding when the vacancies are charged.^{22,73} A more negative charge replacing a halide ion

attracts the Pb²⁺ cations across the vacancy, creating a Pb-Pb species that is stable at both low and ambient temperatures. This mechanism of deep midgap trap formation cannot operate on perovskite surfaces because there is no second Pb atom to create a dimer. This is confirmed by the results depicted in Figure 7, demonstrating three midgap trap states for the bulk vacancy with a charge of -2 and only one shallow state for the surface vacancy with a charge of -2. The trap states can be distinguished by localization in the periodic direction of the slab. Because generation of deep trap levels requires the capture of two electrons, the bulk vacancy defects should be detrimental at high charge carrier densities and benign at low carrier densities. Thus, the surface halide vacancy demonstrates the absence of deep midgap trap states, while the same vacancy in the bulk exhibits multiple deep trap states that can arise from thermal fluctuations and are stabilized by trapped charges.

The absence of deep trap states associated with halide vacancies, a very common point defect, on lead halide surfaces contributes to the bright emission of MHP QDs. 17,74–76 Colloidal QDs made from traditional inorganic semiconductors, such as CdSe, PbS, or Si, 77–79 blink, and the blinking is typically associated with the formation of charged trap states on QD surfaces. The surface vacancy defects do not form deep traps, reducing the rate of blinking. It remains to be seen whether the favorable differences in the properties of point defects in the MHP bulk versus surface persist for other point defects, motivating further investigations. It is important to emphasize that one needs to consider not only optimized structures but also structures sampled at an appropriate temperature, and the fact that proper structure sampling may require long trajectories to capture the slow structural rearrangements of MHPs. 19–21

Slow anharmonic motions play many important roles in MHPs. They induce partial charge carrier localization ^{67,83–88} that rationalizes the unconventional temperature dependence of radiative and nonradiative charge carrier lifetimes; i.e., the lifetimes increase rather than decrease with temperature. ^{84,85,89,90} Geometric distortions of the soft MHP structure give rise to temperature-induced changes in the MHP band gap. ^{16,89,91,92} Anharmonicity relaxes electron—phonon coupling selection rules and allows additional vibrations to couple to the electronic subsystem at higher temperatures. ⁸⁹ This accelerates loss of coherence in the electronic subsystem, and typically, short coherence times favor long excited state lifetimes, ^{93–96} a valuable feature for solar energy and optoelectronic applications. ^{97–99} However, at low temperatures, when anharmonicity is insignificant, coherence times can be very long, ⁷⁴ an important condition for quantum information processing.

In summary, we have demonstrated that halide vacancies can create deep trap states in the bulk of lead halide perovskites; however, no analogous states arise on lead halide perovskite surfaces. The appearance of deep traps requires the formation of a bond between the two Pb atoms across the vacancy, and no such bond can form on the surface. The conclusion applies to both neutral and charged vacancies. Negatively charged vacancies can form stable Pb—Pb dimer species, while neutral vacancies can create the dimers transiently due to large-amplitude thermal fluctuations of the MHP lattice. The transient neutral defects are benign; however, stable charged vacancy defects can be detrimental in the bulk. Because the generation of deep trap states requires the capture of two

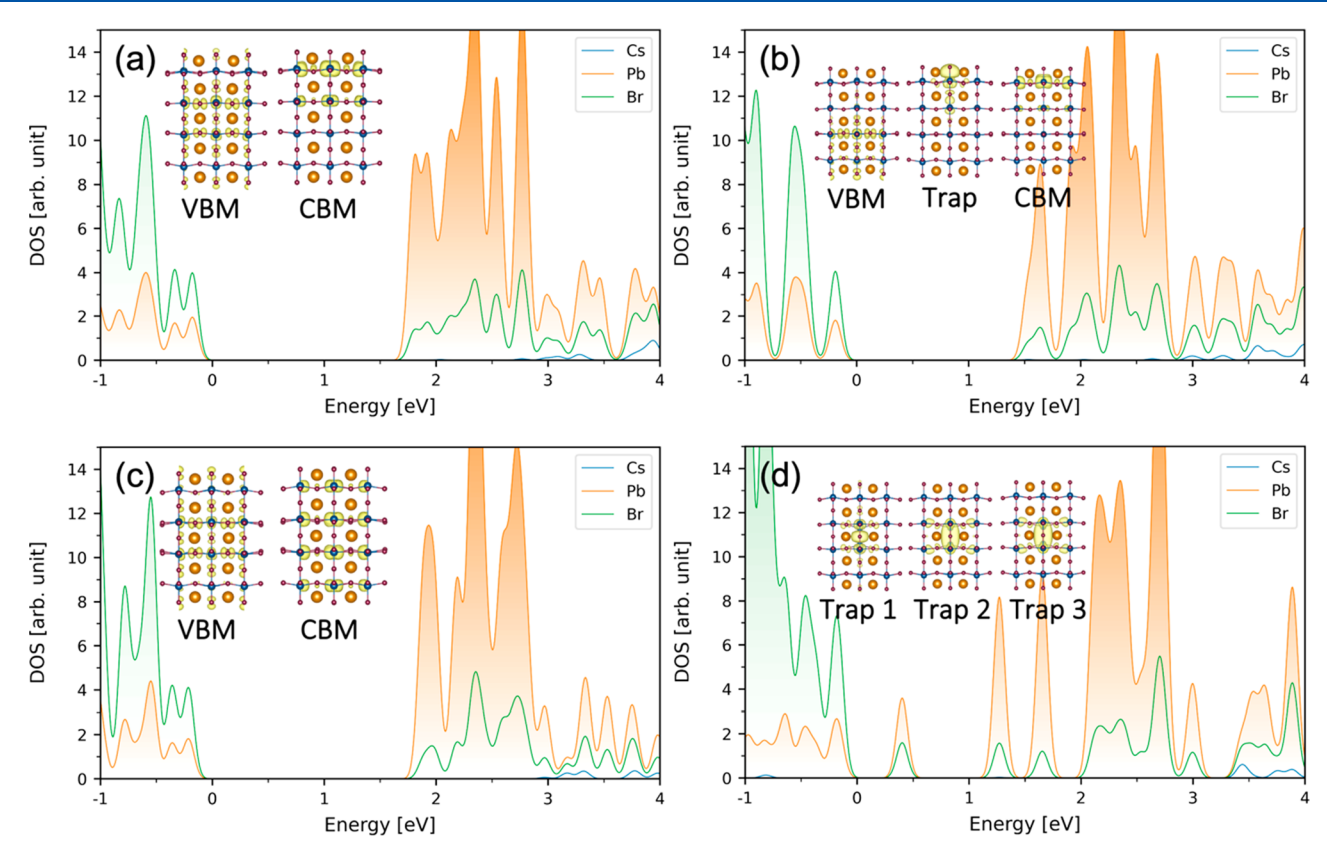


Figure 7. Densities of states of a Br vacancy (a and b) on the $CsPbBr_3$ surface and (c and d) in the $CsPbBr_3$ bulk with added (a and c) -1 and (b and d) -2 charges in the optimized geometries. The insets show the charge densities of the key states. In the -1 state, the vacancies create no midgap trap states at 0 K. The surface vacancy breaks the slab symmetry and results in electron—hole charge separation, like the neutral vacancy at room temperature (Figure 6b,c). Note that there is no electron—hole separation in the neutral surface vacancy at 0 K, as shown in panels e and f of Figure 1. In the -2 state at 0 K, the surface vacancy creates a shallow electron trap (b). However, the bulk vacancy creates three deep midgap traps (d), like the neutral vacancy at room temperature (Figures 3 and 4 and Figure S3). The negative charge attracts the Pb^{2+} cations across the bulk vacancy, creating a stable species.

electrons, the bulk vacancy defects should be detrimental at high charge carrier densities and benign at low carrier densities. The relevant lattice fluctuations occur on a 50-100 ps time scale, and to sample such fluctuations, we have developed a MLFF, trained on the basis of ab initio DFT. As the length of the Pb-Pb bond across the Br vacancy is shortened, up to four trap states can appear inside the CsPbBr₃ band gap. The deepest trap state is formed by the p orbitals of the Pb atoms overlapping to make a σ -bond. The shallow trap states arise from p orbitals of the Pb atoms, forming π -bonds. A halide vacancy on a lead halide perovskite surface breaks the symmetry in the distribution of electron and hole charge densities with the electron being localized at the vacancy on the surface and the hole being localized in the bulk. Although the electron state is supported by the surface vacancy, it is not a trap state, because it is not separated energetically from the conduction band and it is delocalized along the surface. The electron-hole separation facilitated by the surface halide vacancies extends nonradiative and radiative excited state lifetimes. The formation of multiple deep midgap levels in the lead halide perovskite bulk by halide vacancies is possible due to the flexible nature of the lattice that allows large-scale thermal fluctuations and a strong structural response to injected charges. This behavior makes MHPs qualitatively different from traditional inorganic semiconductors that are stiff and undergo minimal structural fluctuations. Halide vacancies are among the most common point defects in

MHPs. The absence of the vacancy-generated trap states on MHP surfaces, combined with the vacancy-induced electron—hole separation, contributes to the excellent optoelectronic properties of MHP QDs that exhibit bright luminescence and slow nonradiative excited state decay without the need for a thorough surface passivation. The absence of charge traps on MHP QD surfaces decreases the rate of blinking, which is common in QDs formed from traditional inorganic semiconductors. The insights provided by this study contribute to the fundamental understanding of MHP properties and help in the development of efficient solar energy and optoelectronic devices.

ASSOCIATED CONTENT

Supporting Information

The Supporting Information is available free of charge at https://pubs.acs.org/doi/10.1021/acs.jpclett.3c01231.

Comparison of potential energies obtained with ab initio calculations and predicted by machine learning, evolution of electronic energy levels, charge densities of the key states in CsPbBr₃ with the bulk Br vacancy showing one, two, and three midgap trap levels, and densities of states of two configurations of CsPbBr₃ with the bulk Br vacancy without midgap trap levels (PDF)

AUTHOR INFORMATION

Corresponding Author

Oleg V. Prezhdo — Department of Chemistry and Department of Physics and Astronomy, University of Southern California, Los Angeles, California 90089, United States; orcid.org/0000-0002-5140-7500; Email: prezhdo@usc.edu

Authors

- Jingyi Ran Department of Chemistry, University of Southern California, Los Angeles, California 90089, United States; orcid.org/0000-0003-0579-7138
- Bipeng Wang Department of Chemistry, University of Southern California, Los Angeles, California 90089, United States; © orcid.org/0000-0003-0924-5867
- **Yifan Wu** Department of Chemistry, University of Southern California, Los Angeles, California 90089, United States
- **Dongyu Liu** *HSE University, 101000 Moscow, Russia;* o orcid.org/0000-0001-6941-1885
- Carlos Mora Perez Department of Chemistry, University of Southern California, Los Angeles, California 90089, United States
- Andrey S. Vasenko HSE University, 101000 Moscow, Russia; I.E. Tamm Department of Theoretical Physics, P.N. Lebedev Physical Institute, Russian Academy of Sciences, 119991 Moscow, Russia; orcid.org/0000-0002-2978-8650

Complete contact information is available at: https://pubs.acs.org/10.1021/acs.jpclett.3c01231

Notes

The authors declare no competing financial interest.

ACKNOWLEDGMENTS

O.V.P. acknowledges the support of the U.S. National Science Foundation via Grant CHE-2154367. A.S.V. acknowledges support from the Mirror Laboratories Project and the Basic Research Program of HSE University.

REFERENCES

- (1) Zhang, W.; Eperon, G. E.; Snaith, H. J. Metal Halide Perovskites for Energy Applications. *Nat. Energy* **2016**, *1*, 16048.
- (2) Shalan, A. E.; Akman, E.; Sadegh, F.; Akin, S. Efficient and Stable Perovskite Solar Cells Enabled by Dicarboxylic Acid-Supported Perovskite Crystallization. *J. Phys. Chem. Lett.* **2021**, *12*, 997–1004.
- (3) Lao, X.; Li, X.; Ågren, H.; Chen, G. Highly Controllable Synthesis and DFT Calculations of Double/Triple-Halide CsPbX₃ (X= Cl, Br, I) Perovskite Quantum Dots: Application to Light-Emitting Diodes. *Nanomaterials* **2019**, *9*, 172.
- (4) Kulkarni, S. A.; Baikie, T.; Boix, P. P.; Yantara, N.; Mathews, N.; Mhaisalkar, S. Band-Gap Tuning of Lead Halide Perovskites Using a Sequential Deposition Process. *Journal of Materials Chemistry A* **2014**, *2*, 9221–9225.
- (5) Unger, E.; Kegelmann, L.; Suchan, K.; Sörell, D.; Korte, L.; Albrecht, S. Roadmap and Roadblocks for the Band Gap Tunability of Metal Halide Perovskites. *Journal of Materials Chemistry A* **2017**, *5*, 11401–11409.
- (6) McGovern, L.; Koschany, I.; Grimaldi, G.; Muscarella, L. A.; Ehrler, B. Grain Size Influences Activation Energy and Migration Pathways in MAPbBr₃ Perovskite Solar Cells. *J. Phys. Chem. Lett.* **2021**, *12*, 2423–2428.
- (7) Gutiérrez Álvarez, S.; Lin, W.; Abdellah, M.; Meng, J.; Zidek, K.; Pullerits, T.; Zheng, K. Charge Carrier Diffusion Dynamics in Multisized Quaternary Alkylammonium-Capped CsPbBr₃ Perovskite Nanocrystal Solids. *ACS Appl. Mater. Interfaces* **2021**, *13*, 44742–44750.

- (8) Herz, L. M. Charge-Carrier Mobilities in Metal Halide Perovskites: Fundamental Mechanisms and Limits. *ACS Energy Letters* **2017**, *2*, 1539–1548.
- (9) Stranks, S. D.; Eperon, G. E.; Grancini, G.; Menelaou, C.; Alcocer, M. J.; Leijtens, T.; Herz, L. M.; Petrozza, A.; Snaith, H. J. Electron-Hole Diffusion Lengths Exceeding 1 Micrometer in an Organometal Trihalide Perovskite Absorber. *Science* **2013**, 342, 341–344.
- (10) Noh, J. H.; Im, S. H.; Heo, J. H.; Mandal, T. N.; Seok, S. I. Chemical Management for Colorful, Efficient, and Stable Inorganic—Organic Hybrid Nanostructured Solar Cells. *Nano Lett.* **2013**, *13*, 1764—1769.
- (11) Saliba, M.; Matsui, T.; Domanski, K.; Seo, J.-Y.; Ummadisingu, A.; Zakeeruddin, S. M.; Correa-Baena, J.-P.; Tress, W. R.; Abate, A.; Hagfeldt, A.; Grätzel, M. Incorporation of Rubidium Cations into Perovskite Solar Cells Improves Photovoltaic Performance. *Science* **2016**, 354, 206–209.
- (12) Zhang, J. B.; Yin, C. Y.; Yang, F.; Yao, Y.; Yuan, F. L.; Chen, H. T.; Wang, R. W.; Bai, S.; Tu, G. L.; Hou, L. T. Highly Luminescent and Stable CsPbI₃ Perovskite Nanocrystals with Sodium Dodecyl Sulfate Ligand Passivation for Red-Light-Emitting Diodes. *J. Phys. Chem. Lett.* **2021**, *12*, 2437–2443.
- (13) Kim, M.; Jeong, J.; Lu, H. Z.; Lee, T. K.; Eickemeyer, F. T.; Liu, Y. H.; Choi, I. W.; Choi, S. J.; Jo, Y.; Kim, H. B.; Mo, S. I.; Kim, Y. K.; Lee, H.; An, N. G.; Cho, S.; Tress, W. R.; Zakeeruddin, S. M.; Hagfeldt, A.; Kim, J. Y.; Gratzel, M.; Kim, D. S. Conformal Quantum Dot-SnO₂ Layers as Electron Transporters for Efficient Perovskite Solar Cells. *Science* 2022, 375, 302–306.
- (14) Jiang, Y. Z.; Wei, J. L.; Yuan, M. J. Energy-Funneling Process in Quasi-2d Perovskite Light-Emitting Diodes. *J. Phys. Chem. Lett.* **2021**, 12, 2593–2606.
- (15) Cheng, S. J.; Zhong, H. Z. What Happens When Halide Perovskites Meet with Water? *J. Phys. Chem. Lett.* **2022**, *13*, 2281–2290.
- (16) Marronnier, A.; Roma, G.; Boyer-Richard, S.; Pedesseau, L.; Jancu, J.-M.; Bonnassieux, Y.; Katan, C.; Stoumpos, C. C.; Kanatzidis, M. G.; Even, J. Anharmonicity and Disorder in the Black Phases of Cesium Lead Iodide Used for Stable Inorganic Perovskite Solar Cells. *ACS Nano* **2018**, *12*, 3477–3486.
- (17) Protesescu, L.; Yakunin, S.; Bodnarchuk, M. I.; Krieg, F.; Caputo, R.; Hendon, C. H.; Yang, R. X.; Walsh, A.; Kovalenko, M. V. Nanocrystals of Cesium Lead Halide Perovskites (CsPbX₃, X = Cl, Br, and I): Novel Optoelectronic Materials Showing Bright Emission with Wide Color Gamut. *Nano Lett.* **2015**, *15*, 3692–3696.
- (18) Cohen, A. V.; Egger, D. A.; Rappe, A. M.; Kronik, L. Breakdown of the Static Picture of Defect Energetics in Halide Perovskites: The Case of the Br Vacancy in CsPbBr₃. *J. Phys. Chem. Lett.* **2019**, *10*, 4490–4498.
- (19) Wang, B.; Chu, W.; Wu, Y.; Casanova, D.; Saidi, W. A.; Prezhdo, O. V. Electron-Volt Fluctuation of Defect Levels in Metal Halide Perovskites on a 100 Ps Time Scale. *J. Phys. Chem. Lett.* **2022**, 13, 5946–5952.
- (20) Wu, Y.; Liu, D.; Chu, W.; Wang, B.; Vasenko, A. S.; Prezhdo, O. V. Fluctuations at Metal Halide Perovskite Grain Boundaries Create Transient Trap States: Machine Learning Assisted Ab Initio Analysis. ACS Appl. Mater. Interfaces 2022, 14, 55753-55761.
- (21) Liu, D.; Wu, Y.; Vasenko, A. S.; Prezhdo, O. V. Grain Boundary Sliding and Distortion on a Nanosecond Timescale Induce Trap States in CsPbBr₃: Ab Initio Investigation with Machine Learning Force Field. *Nanoscale* **2022**, *15*, 285–293.
- (22) Li, W.; Liu, J.; Bai, F.-Q.; Zhang, H.-X.; Prezhdo, O. V. Hole Trapping by Iodine Interstitial Defects Decreases Free Carrier Losses in Perovskite Solar Cells: A Time-Domain Ab Initio Study. ACS Energy Letters 2017, 2, 1270–1278.
- (23) Li, W.; Sun, Y.-Y.; Li, L.; Zhou, Z.; Tang, J.; Prezhdo, O. V. Control of Charge Recombination in Perovskites by Oxidation State of Halide Vacancy. *J. Am. Chem. Soc.* **2018**, *140*, 15753–15763.

- (24) Chu, W.; Saidi, W. A.; Zhao, J.; Prezhdo, O. V. Soft Lattice and Defect Covalency Rationalize Tolerance of B-CsPbI₃ Perovskite Solar Cells to Native Defects. *Angew. Chem., Int. Ed.* **2020**, *59*, 6435–6441.
- (25) Chu, W.; Zheng, Q.; Prezhdo, O. V.; Zhao, J.; Saidi, W. A. Low-Frequency Lattice Phonons in Halide Perovskites Explain High Defect Tolerance toward Electron-Hole Recombination. *Sci. Adv.* **2020**, *6*, eaaw7453.
- (26) Li, W.; Long, R.; Tang, J.; Prezhdo, O. V. Influence of Defects on Excited-State Dynamics in Lead Halide Perovskites: Time-Domain Ab Initio Studies. *J. Phys. Chem. Lett.* **2019**, *10*, 3788–3804.
- (27) Li, W.; She, Y.; Vasenko, A. S.; Prezhdo, O. V. Ab Initio Nonadiabatic Molecular Dynamics of Charge Carriers in Metal Halide Perovskites. *Nanoscale* **2021**, *13*, 10239–10265.
- (28) Yin, W. J.; Shi, T. T.; Yan, Y. F. Unusual Defect Physics in CH₃NH₃PbI₃ Perovskite Solar Cell Absorber. *Appl. Phys. Lett.* **2014**, 104, 063903.
- (29) Chang, T.; Wei, Q. L.; Zeng, R. S.; Cao, S.; Zhao, J. L.; Zou, B. S. Efficient Energy Transfer in Te⁴⁺-Doped Cs₃ZrCl₆ Vacancy-Ordered Perovskites and Ultrahigh Moisture Stability Via a-Site Rb-Alloying Strategy. *J. Phys. Chem. Lett.* **2021**, *12*, 1829–1837.
- (30) Wright, A. D.; Buizza, L. R. V.; Savill, K. J.; Longo, G.; Snaith, H. J.; Johnston, M. B.; Herz, L. M. Ultrafast Excited-State Localization in Cs₂AgBiBr₆ Double Perovskite. *J. Phys. Chem. Lett.* **2021**, *12*, 3352–3360.
- (31) Frost, J. M.; Butler, K. T.; Brivio, F.; Hendon, C. H.; van Schilfgaarde, M.; Walsh, A. Atomistic Origins of High-Performance in Hybrid Halide Perovskite Solar Cells. *Nano Lett.* **2014**, *14*, 2584–2590
- (32) Liu, D. Y.; Perez, C. M.; Vasenko, A. S.; Prezhdo, O. V. Ag-Bi Charge Redistribution Creates Deep Traps in Defective Cs₂AgBiBr₆: Machine Learning Analysis of Density Functional Theory. *J. Phys. Chem. Lett.* **2022**, *13*, 3645–3651.
- (33) Chu, W. B.; Saidi, W. A.; Prezhdo, O. V. Long-Lived Hot Electron in a Metallic Particle for Plasmonics and Catalysis: Ab Initio Nonadiabatic Molecular Dynamics with Machine Learning. *ACS Nano* **2020**, *14*, 10608–10615.
- (34) Schleder, G. R.; Padilha, A. C.; Acosta, C. M.; Costa, M.; Fazzio, A. From DFT to Machine Learning: Recent Approaches to Materials Science—A Review. *Journal of Physics: Materials* **2019**, *2*, No. 032001.
- (35) Gu, G. H.; Noh, J.; Kim, I.; Jung, Y. Machine Learning for Renewable Energy Materials. *Journal of Materials Chemistry A* **2019**, *7*, 17096–17117.
- (36) Huan, T. D.; Batra, R.; Chapman, J.; Krishnan, S.; Chen, L.; Ramprasad, R. A Universal Strategy for the Creation of Machine Learning-Based Atomistic Force Fields. *npj Comput. Mater.* **2017**, 3, 27
- (37) Butler, K. T.; Davies, D. W.; Cartwright, H.; Isayev, O.; Walsh, A. Machine Learning for Molecular and Materials Science. *Nature* **2018**, *559*, 547–555.
- (38) Ouyang, Y.; Yu, C.; He, J.; Jiang, P.; Ren, W.; Chen, J. Accurate Description of High-Order Phonon Anharmonicity and Lattice Thermal Conductivity from Molecular Dynamics Simulations with Machine Learning Potential. *Phys. Rev. B* **2022**, *105*, 115202.
- (39) Mortazavi, B.; Podryabinkin, E. V.; Novikov, I. S.; Rabczuk, T.; Zhuang, X.; Shapeev, A. V. Accelerating First-Principles Estimation of Thermal Conductivity by Machine-Learning Interatomic Potentials: A MTP/ShengBTE Solution. *Comput. Phys. Commun.* **2021**, 258, 107583.
- (40) Zong, H.; Pilania, G.; Ding, X.; Ackland, G. J.; Lookman, T. Developing an Interatomic Potential for Martensitic Phase Transformations in Zirconium by Machine Learning. *npj Comput. Mater.* **2018**, *4*, 48.
- (41) Li, L.; Yang, Y.; Zhang, D.; Ye, Z.-G.; Jesse, S.; Kalinin, S. V.; Vasudevan, R. K. Machine Learning-Enabled Identification of Material Phase Transitions Based on Experimental Data: Exploring Collective Dynamics in Ferroelectric Relaxors. *Sci. Adv.* **2018**, *4*, eaap8672.

- (42) Meuwly, M. Machine Learning for Chemical Reactions. *Chem. Rev.* **2021**, *121*, 10218–10239.
- (43) Westermayr, J.; Gastegger, M.; Marquetand, P. Combining Schnet and Sharc: The Schnarc Machine Learning Approach for Excited-State Dynamics. *journal of physical chemistry letters* **2020**, *11*, 3828–3834.
- (44) Kim, C.; Pilania, G.; Ramprasad, R. From Organized High-Throughput Data to Phenomenological Theory Using Machine Learning: The Example of Dielectric Breakdown. *Chem. Mater.* **2016**, *28*, 1304–1311.
- (45) Poltavsky, I.; Tkatchenko, A. Machine Learning Force Fields: Recent Advances and Remaining Challenges. *J. Phys. Chem. Lett.* **2021**, *12*, 6551–6564.
- (46) Kang, J.; Wang, L.-W. High Defect Tolerance in Lead Halide Perovskite CsPbBr₃. journal of physical chemistry letters **2017**, 8, 489–493.
- (47) Yin, J.; Yang, H.; Song, K.; El-Zohry, A. M.; Han, Y.; Bakr, O. M.; Brédas, J.-L.; Mohammed, O. F. Point Defects and Green Emission in Zero-Dimensional Perovskites. *J. Phys. Chem. Lett.* **2018**, 9, 5490–5495.
- (48) Kresse, G.; Hafner, J. Ab initio molecular dynamics for liquid metals. Phys. Rev. B 1993, 47, 558.
- (49) Perdew, J. P.; Burke, K.; Ernzerhof, M. Generalized Gradient Approximation Made Simple. *Physical review letters* **1996**, 77, 3865.
- (50) Kresse, G.; Joubert, D. From Ultrasoft Pseudopotentials to the Projector Augmented-Wave Method. *Physical review b* **1999**, *59*, 1758.
- (51) Momma, K.; Izumi, F. Vesta 3 for Three-Dimensional Visualization of Crystal, Volumetric and Morphology Data. *J. Appl. Crystallogr.* **2011**, *44*, 1272–1276.
- (52) Oksenberg, E.; Sanders, E.; Popovitz-Biro, R.; Houben, L.; Joselevich, E. Surface-Guided CsPbBr₃ Perovskite Nanowires on Flat and Faceted Sapphire with Size-Dependent Photoluminescence and Fast Photoconductive Response. *Nano Lett.* **2018**, *18*, 424–433.
- (53) Ma, S.; Kim, S. H.; jeong, B.; Kwon, H. C.; Yun, S. C.; Jang, G.; Yang, H.; Park, C.; Lee, D.; Moon, J. Strain-Mediated Phase Stabilization: A New Strategy for Ultrastable Alpha-CsPbI₃ Perovskite by Nanoconfined Growth. *Small* **2019**, *15*, 1900219.
- (54) Ezzeldien, M.; Al-Qaisi, S.; Alrowaili, Z. A.; Alzaid, M.; Maskar, E.; Es-Smairi, A.; Vu, T. V.; Rai, D. P. Electronic and Optical Properties of Bulk and Surface of CsPbBr₃ Inorganic Halide Perovskite a First Principles DFT 1/2 Approach. *Sci. Rep.* **2021**, *11*, 20622.
- (55) Yang, Y.; Hou, C. J.; Liang, T. X. Energetic and Electronic Properties of CsPbBr₃ Surfaces: A First-Principles Study. *Phys. Chem. Chem. Phys.* **2021**, 23, 7145–7152.
- (56) Wang, H.; Zhang, L.; Han, J.; Weinan, E. Deepmd-Kit: A Deep Learning Package for Many-Body Potential Energy Representation and Molecular Dynamics. *Comput. Phys. Commun.* **2018**, 228, 178–184.
- (57) Plimpton, S. Fast Parallel Algorithms for Short-Range Molecular Dynamics. *J. Comput. Phys.* **1995**, *117*, 1–19.
- (58) Yuan, Y. B.; Huang, J. S. Ion Migration in Organometal Trihalide Perovskite and Its Impact on Photovoltaic Efficiency and Stability. *Acc. Chem. Res.* **2016**, *49*, 286–293.
- (59) Bischak, C. G.; Hetherington, C. L.; Wu, H.; Aloni, S.; Ogletree, D. F.; Limmer, D. T.; Ginsberg, N. S. Origin of Reversible Photoinduced Phase Separation in Hybrid Perovskites. *Nano Lett.* **2017**, *17*, 1028–1033.
- (60) Jokar, E.; Chuang, H. S.; Kuan, C. H.; Wu, H. P.; Hou, C. H.; Shyue, J. J.; Diau, E. W. G. Slow Passivation and Inverted Hysteresis for Hybrid Tin Perovskite Solar Cells Attaining 13.5% Via Sequential Deposition. *J. Phys. Chem. Lett.* **2021**, *12*, 10106–10111.
- (61) Tong, C. J.; Geng, W.; Prezhdo, O. V.; Liu, L. M. Role of Methylammonium Orientation in Ion Diffusion and Current Voltage Hysteresis in the CH₃NH₃PbI₃ Perovskite. *Acs Energy Letters* **2017**, *2*, 1997–2004.
- (62) Tong, C. J.; Li, L. Q.; Liu, L. M.; Prezhdo, O. V. Synergy between Ion Migration and Charge Carrier Recombination in Metal-Halide Perovskites. *J. Am. Chem. Soc.* **2020**, *142*, 3060–3068.

- (63) Shi, R.; Fang, W. H.; Vasenko, A. S.; Long, R.; Prezhdo, O. V. Efficient Passivation of Dy Center in CH₃NH₃PbBr₃ by Chlorine: Quantum Molecular Dynamics. *Nano Research* **2022**, *15*, 2112–2122.
- (64) Neutzner, S.; Thouin, F.; Cortecchia, D.; Petrozza, A.; Silva, C.; Srimath Kandada, A. R. Exciton-Polaron Spectral Structures in Two-Dimensional Hybrid Lead-Halide Perovskites. *Phys. Rev. Mater.* **2018**, 2, No. 064605.
- (65) Lang, F.; Shargaieva, O.; Brus, V. V.; Neitzert, H. C.; Rappich, J.; Nickel, N. H. Influence of Radiation on the Properties and the Stability of Hybrid Perovskites. *Adv. Mater.* **2018**, *30*, 1702905.
- (66) Straus, D. B.; Kagan, C. R. Electrons, Excitons, and Phonons in Two-Dimensional Hybrid Perovskites: Connecting Structural, Optical, and Electronic Properties. *journal of physical chemistry letters* **2018**, 9, 1434–1447.
- (67) Zhang, Z.; Fang, W.-H.; Long, R.; Prezhdo, O. V. Exciton Dissociation and Suppressed Charge Recombination at 2D Perovskite Edges: Key Roles of Unsaturated Halide Bonds and Thermal Disorder. J. Am. Chem. Soc. 2019, 141, 15557–15566.
- (68) Shi, R.; Vasenko, A. S.; Long, R.; Prezhdo, O. V. Edge Influence on Charge Carrier Localization and Lifetime in CH₃NH₃PbBr₃ Perovskite: Ab Initio Quantum Dynamics Simulation. *J. Phys. Chem. Lett.* **2020**, *11*, 9100–9109.
- (69) He, J. L.; Fang, W. H.; Long, R.; Prezhdo, O. V. Bidentate Lewis Bases Are Preferred for Passivation of MAPbI₃ Surfaces: A Time-Domain Ab Initio Analysis. *Nano Energy* **2021**, *79*, 105491.
- (70) Zhao, X.; Vasenko, A. S.; Prezhdo, O. V.; Long, R. Anion Doping Delays Nonradiative Electron-Hole Recombination in Cs-Based All-Inorganic Perovskites: Time Domain Ab Initio Analysis. *J. Phys. Chem. Lett.* **2022**, *13*, 11375–11382.
- (71) Shi, R.; Long, R.; Fang, W. H.; Prezhdo, O. V. Rapid Interlayer Charge Separation and Extended Carrier Lifetimes Due to Spontaneous Symmetry Breaking in Organic and Mixed Organic-Inorganic Dion-Jacobson Perovskites. *J. Am. Chem. Soc.* **2023**, *145*, 5297–5309.
- (72) Liu, L. H.; Fang, W. H.; Long, R.; Prezhdo, O. V. Lewis Base Passivation of Hybrid Halide Perovskites Slows Electron-Hole Recombination: Time-Domain Ab Lnitio Analysis. *J. Phys. Chem. Lett.* **2018**, *9*, 1164–1171.
- (73) Agiorgousis, M. L.; Sun, Y. Y.; Zeng, H.; Zhang, S. B. Strong Covalency-Induced Recombination Centers in Perovskite Solar Cell Material CH₃NH₃PbI₃. *J. Am. Chem. Soc.* **2014**, *136*, 14570–14575.
- (74) Utzat, H.; Sun, W. W.; Kaplan, A. E. K.; Krieg, F.; Ginterseder, M.; Spokoyny, B.; Klein, N. D.; Shulenberger, K. E.; Perkinson, C. F.; Kovalenko, M. V.; Bawendi, M. G. Coherent Single-Photon Emission from Colloidal Lead Halide Perovskite Quantum Dots. *Science* 2019, 363, 1068.
- (75) Akkerman, Q. A.; Raino, G.; Kovalenko, M. V.; Manna, L. Genesis, Challenges and Opportunities for Colloidal Lead Halide Perovskite Nanocrystals. *Nat. Mater.* **2018**, *17*, 394–405.
- (76) Swarnkar, A.; Chulliyil, R.; Ravi, V. K.; Irfanullah, M.; Chowdhury, A.; Nag, A. Colloidal CsPbBr₃ Perovskite Nanocrystals: Luminescence Beyond Traditional Quantum Dots. *Angew. Chem., Int. Ed.* **2015**, *54*, 15424–15428.
- (77) Alivisatos, A. P. Semiconductor Clusters, Nanocrystals, and Quantum Dots. *Science* **1996**, *271*, 933–937.
- (78) Prezhdo, O. V. Multiple Excitons and the Electron-Phonon Bottleneck in Semiconductor Quantum Dots: An Ab Initio Perspective. *Chem. Phys. Lett.* **2008**, *460*, 1–9.
- (79) Hyeon-Deuk, K.; Prezhdo, O. V. Multiple Exciton Generation and Recombination Dynamics in Small Si and CdSe Quantum Dots: An Ab Initio Time-Domain Study. ACS Nano 2012, 6, 1239–1250.
- (80) Chen, O.; Zhao, J.; Chauhan, V. P.; Cui, J.; Wong, C.; Harris, D. K.; Wei, H.; Han, H. S.; Fukumura, D.; Jain, R. K.; Bawendi, M. G. Compact High-Quality CdSe-CdS Core-Shell Nanocrystals with Narrow Emission Linewidths and Suppressed Blinking. *Nat. Mater.* **2013**, *12*, 445–451.
- (81) Houtepen, A. J.; Hens, Z.; Owen, J. S.; Infante, I. On the Origin of Surface Traps in Colloidal Ii-Vi Semiconductor Nanocrystals. *Chem. Mater.* **2017**, 29, 752–761.

- (82) Trivedi, D. J.; Wang, L. J.; Prezhdo, O. V. Auger-Mediated Electron Relaxation Is Robust to Deep Hole Traps: Time-Domain Ab Initio Study of CdSe Quantum Dots. *Nano Lett.* **2015**, *15*, 2086–2091.
- (83) Li, W.; Vasenko, A. S.; Tang, J.; Prezhdo, O. V. Anharmonicity Extends Carrier Lifetimes in Lead Halide Perovskites at Elevated Temperatures. *J. Phys. Chem. Lett.* **2019**, *10*, 6219–6226.
- (84) Zhou, G.; Chu, W.; Prezhdo, O. V. Structural Deformation Controls Charge Losses in MAPbI₃: Unsupervised Machine Learning of Nonadiabatic Molecular Dynamics. *ACS Energy Letters* **2020**, *S*, 1930–1938.
- (85) Mangan, S. M.; Zhou, G.; Chu, W.; Prezhdo, O. V. Dependence between Structural and Electronic Properties of CsPbI₃: Unsupervised Machine Learning of Nonadiabatic Molecular Dynamics. *J. Phys. Chem. Lett.* **2021**, *12*, 8672–8678.
- (86) Aristidou, N.; Eames, C.; Sanchez-Molina, I.; Bu, X.; Kosco, J.; Islam, M. S.; Haque, S. A. Fast Oxygen Diffusion and Iodide Defects Mediate Oxygen-Induced Degradation of Perovskite Solar Cells. *Nat. Commun.* **2017**, *8*, 15218.
- (87) He, J.; Fang, W.-H.; Long, R.; Prezhdo, O. V. Superoxide/ Peroxide Chemistry Extends Charge Carriers' Lifetime but Undermines Chemical Stability of CH₃NH₃PbI₃ Exposed to Oxygen: Time-Domain Ab Initio Analysis. *J. Am. Chem. Soc.* **2019**, *141*, 5798–5807.
- (88) Zhang, Z.; Fang, W.-H.; Tokina, M. V.; Long, R.; Prezhdo, O. V. Rapid Decoherence Suppresses Charge Recombination in Multi-Layer 2D Halide Perovskites: Time-Domain Ab Initio Analysis. *Nano Lett.* **2018**, *18*, 2459–2466.
- (89) Li, W.; Tang, J.; Casanova, D.; Prezhdo, O. V. Time-Domain Ab Initio Analysis Rationalizes the Unusual Temperature Dependence of Charge Carrier Relaxation in Lead Halide Perovskite. *ACS Energy Letters* **2018**, *3*, 2713–2720.
- (90) Li, W.; Chen, Z.; Tang, J.; Prezhdo, O. V. Anti-Correlation between Band Gap and Carrier Lifetime in Lead Halide Perovskites under Compression Rationalized by Ab Initio Quantum Dynamics. *Chem. Mater.* **2020**, 32, 4707–4715.
- (91) Patrick, C. E.; Jacobsen, K. W.; Thygesen, K. S. Anharmonic Stabilization and Band Gap Renormalization in the Perovskite CsSnI₃. *Phys. Rev. B* **2015**, *92*, 201205.
- (92) Long, R.; Fang, Q.; Vasenko, A. S.; Shi, R.; Fang, W. H.; Prezhdo, O. V. Structural Disorder in Higher-Temperature Phases Increases Charge Carrier Lifetimes in Metal Halide Perovskites. *J. Am. Chem. Soc.* **2022**, *144*, 19137–19149.
- (93) Akimov, A. V.; Prezhdo, O. V. Persistent Electronic Coherence Despite Rapid Loss of Electron-Nuclear Correlation. *J. Phys. Chem. Lett.* **2013**, *4*, 3857–3864.
- (94) Kilina, S. V.; Neukirch, A. J.; Habenicht, B. F.; Kilin, D. S.; Prezhdo, O. V. Quantum Zeno Effect Rationalizes the Phonon Bottleneck in Semiconductor Quantum Dots. *Phys. Rev. Lett.* **2013**, *110*, 180404.
- (95) Itano, W. M.; Heinzen, D. J.; Bollinger, J. J.; Wineland, D. J. Quantum Zeno Effect. *Phys. Rev. A* **1990**, *41*, 2295–2300.
- (96) Kamisaka, H.; Kilina, S. V.; Yamashita, K.; Prezhdo, O. V. Ultrafast Vibrationally-Induced Dephasing of Electronic Excitations in PbSe Quantum Dot. *Nano Lett.* **2006**, *6*, 2295–2300.
- (97) Li, X.; Cao, F.; Yu, D.; Chen, J.; Sun, Z.; Shen, Y.; Zhu, Y.; Wang, L.; Wei, Y.; Wu, Y.; Zeng, H. All Inorganic Halide Perovskites Nanosystem: Synthesis, Structural Features, Optical Properties and Optoelectronic Applications. *Small* **2017**, *13*, 1603996.
- (98) Fu, Y.; Zhu, H.; Chen, J.; Hautzinger, M. P.; Zhu, X.-Y.; Jin, S. Metal Halide Perovskite Nanostructures for Optoelectronic Applications and the Study of Physical Properties. *Nature Reviews Materials* **2019**, *4*, 169–188.
- (99) Zhao, Y.; Zhu, K. Organic–Inorganic Hybrid Lead Halide Perovskites for Optoelectronic and Electronic Applications. *Chem. Soc. Rev.* **2016**, 45, 655–689.